

Physicochemical Properties of Potential Cathode $\text{La}_{1-x}\text{Ba}_x\text{Mn}_{1-y}\text{Cr}_y\text{O}_3$ and Anode $\text{Sr}_2\text{NiMoO}_6$ Materials for Solid-Oxide Fuel Cells

Filonova E.A.* and Dmitriev A.S.

Ural Federal University named after the first President of Russia B.N. Yeltsin,
Yekaterinburg, Lenin Av., 51, Russia

Abstract

The homogeneity area boundaries of $\text{La}_{1-x}\text{Ba}_x\text{Mn}_{1-y}\text{Cr}_y\text{O}_3$ solid solutions possessing orthorhombic and rhombohedral structures were established. A state diagram at 1373 K in air in the quaternary oxide system $\text{LaMnO}_3\text{-BaMnO}_3\text{-BaCrO}_4\text{-LaCrO}_3$ was drawn for the first time. Partial substitution of Mn with Cr in $\text{La}_{1-x}\text{Ba}_x\text{MnO}_3$ stored the thermal compatibility of the cathode with the any traditionally used electrolyte but reduced the electric conductivity of the potential cathode. Based on the linear lengthening measurements of $\text{La}_{1-x}\text{Ba}_x\text{Mn}_{1-y}\text{Cr}_y\text{O}_3$ and $\text{Sr}_2\text{NiMoO}_6$ samples the values of the thermal expansion coefficients were calculated. It was established that the temperature of the structure transition from a tetragonal to a cubic phase in $\text{Sr}_2\text{NiMoO}_6$ occurred at 508 K. It was stated that double perovskite $\text{Sr}_2\text{NiMoO}_6$ in air did not react with $(\text{La}_{0.9}\text{Sr}_{0.1})_{0.98}\text{Ga}_{0.8}\text{Mg}_{0.2}\text{O}_3$ up to 1073 K.

Introduction

The development and investigation of various materials for solid-oxide fuel cells (SOFCs) is now an increasingly popular research area in physical chemistry. Conventional SOFCs use $\text{Y}_{2x}\text{Zr}_{1-2x}\text{O}_{2-x}$ (YSZ) as the electrolyte, $\text{La}_{1-x}\text{Sr}_x\text{MnO}_3$ as the cathode, and metallic Ni as the anode [1].

The traditionally used $\text{La}_{1-x}\text{Sr}_x\text{MnO}_3$ manganite is the best cathode for high-temperature uses (1073-1273 K) giving the stable electric contact to the YSZ as electrolyte material [1]. Today only one problem threatens to the long-term stability of $\text{La}_{1-x}\text{Sr}_x\text{MnO}_3$ as cathode. It is diffusion of the cations under the influence of the oxygen chemical potential gradient which leads to the decomposition of the oxide [2]. Having the higher values of the electrical conductivity $\text{La}_{1-x}\text{Sr}_x\text{CoO}_3$ and $\text{La}_{1-x}\text{Sr}_x\text{FeO}_3$ at high temperatures react with YSZ electrolyte with the $\text{La}_2\text{Zr}_2\text{O}_7$ or SrZrO_3 phase formation that resulted in significant current increasing [1].

The traditionally used Ni anode has the high catalytic activity in the reactions of the hydrocarbons conversion and in the reactions of the hydrogen and CO oxidation but is not compatible at high temperatures with YSZ electrolyte material due to the difference in the thermal expansion coefficients [1]. For overcoming of this lack the nickel powder is mixed with YSZ particles obtaining the Ni-YSZ composite (cermet) but this anode is strongly fouled by carbon deposition and sulfur poisoning when operated with natural gas [3].

To avoid the problems of the oxides stability and the differences in the thermal expansion coefficients of the various parts of SOFCs investigators tried to decrease the working temperatures of SOFCs that led to the necessity of YSZ as electrolyte material on $\text{La}_{0.9}\text{Sr}_{0.1}\text{Ga}_{0.8}\text{Mg}_{0.2}\text{O}_{2.85}$ [4]. In comparison with YSZ $\text{La}_{0.9}\text{Sr}_{0.1}\text{Ga}_{0.8}\text{Mg}_{0.2}\text{O}_{2.85}$ has the higher value of electric conductivity but in this case there is impossible to use the nickel anode due to chemical interaction.

All these problems constrain practical applications of SOFCs and highlight the need for

*corresponding author. Email: helen.filonova@usu.ru

further research of other oxide systems that can be used as the cathode and anode materials.

The aim of this paper was to determine the influence of the dopant concentration of *Cr* (*Cr*-doping sufficiently increased the thermodynamic stability of oxide material [5]) to on the crystal structure and thermal expansion of *Ba*-doped LaMnO_3 estimating those utility of *Cr*-doped $\text{La}_{1-x}\text{Ba}_x\text{MnO}_3$ as a potential cathode material. Earlier, we reported the crystal structure and physical-chemical properties of solid solutions of $\text{La}_{1-x}\text{Ba}_x\text{MnO}_3$ [6] and $\text{La}_{1-x}\text{Ba}_x\text{Mn}_{1-y}\text{Co}_{1-y}\text{O}_3$ [7]. To compare the thermal expansion of various parts of SOFCs we also investigated the thermal and the chemical stability of double perovskite $\text{Sr}_2\text{NiMoO}_6$. It was informed that $\text{Sr}_2\text{NiMoO}_6$ may represent a perspective new anode material owing to the high oxide-ion/electron conductivity and the compatibility with $\text{La}_{0.9}\text{Sr}_{0.1}\text{Ga}_{0.8}\text{Mg}_{0.2}\text{O}_{2.85}$ electrolyte both [8].

Experimental

Samples of $\text{La}_{1-x}\text{Ba}_x\text{Mn}_{1-y}\text{Cr}_y\text{O}_3$ were synthesized using the standard ceramic technique described in [7].

The $\text{Sr}_2\text{NiMoO}_6$ sample was obtained by the self-propagation method using precursor solutions. Stoichiometric amounts of “special purity” grade SrCO_3 and “pure for analysis” grade $\text{Ni}(\text{CH}_3\text{COO})_2 \cdot 4\text{H}_2\text{O}$ were first dissolved in diluted nitric acid and then mixed with “chemical purity” grade $(\text{NH}_4)_6\text{Mo}_7\text{O}_{24} \cdot 4\text{H}_2\text{O}$. Prior to this, contents of crystal-lattice water were determined for the starting materials by atomic emission spectroscopic analysis. A water solution of polyvinyl alcohol was added to the precursor solution as an organic fuel. The solution was evaporated on a hot plate, and the powder was then calcined in five steps at 1073–1373 K in air for 24 h in the first and the second step and for 48 h in the third one.

To measure the physical properties, the $\text{La}_{1-x}\text{Ba}_x\text{Mn}_{1-y}\text{Cr}_y\text{O}_3$ and $\text{Sr}_2\text{NiMoO}_6$ powders were pressed into bars $3 \times 4 \times 23$ mm and finally sintered at 1573 K in air for 24 h.

To study the chemical compatibility, the electrolytes $\text{Ce}_{0.8}\text{Sm}_{0.2}\text{O}_{2-\delta}$ and $(\text{La}_{0.9}\text{Sr}_{0.1})_{0.98}\text{Ga}_{0.8}\text{Mg}_{0.2}\text{O}_3$ were synthesized by the self-propagation method from “pure for analysis” grade $\text{Ce}(\text{NO}_3)_3 \cdot 6\text{H}_2\text{O}$, Sm_2O_3 (99.99%) and “chemical purity” grade $\text{La}(\text{NO}_3)_3 \cdot 6\text{H}_2\text{O}$, “special purity” grade SrCO_3 , “pure for analysis” MgO , Ga (99.99%) respectively. Stoichiometric amounts of starting

materials were dissolved in diluted nitric acid. Glycerine or glycin was added to the precursor solutions as an organic agent. The solutions were evaporated on a hot plate, and the powders were then calcined in three 24 h steps in air at 673–1373 K for $\text{Ce}_{0.8}\text{Sm}_{0.2}\text{O}_{2-\delta}$ and at 873–1573 K for $(\text{La}_{0.9}\text{Sr}_{0.1})_{0.98}\text{Ga}_{0.8}\text{Mg}_{0.2}\text{O}_3$. The electrolyte $\text{Zr}_{0.85}\text{Y}_{0.15}\text{O}_2$ was synthesized by the cooperate precipitation technique from ‘pure for analysis’ grade $\text{Zr}(\text{OH})_2\text{CO}_3 \cdot \text{H}_2\text{O}$ and ‘pure for analysis’ grade Y_2O_3 . Stoichiometric amounts of starting materials were dissolved in diluted nitric acid and then mixed with NH_4OH . The obtained precipitate was annealed firstly at 373 K for 6h in air and finally at 973 K for 10 h.

The phase purity and the lattice parameters of the $\text{La}_{1-x}\text{Ba}_x\text{Mn}_{1-y}\text{Cr}_y\text{O}_3$ and the $\text{Sr}_2\text{NiMoO}_6$ samples and the phase purity of $\text{Ce}_{0.8}\text{Sm}_{0.2}\text{O}_{2-\delta}$, $\text{Zr}_{0.85}\text{Y}_{0.15}\text{O}_2$, $(\text{La}_{0.9}\text{Sr}_{0.1})_{0.98}\text{Ga}_{0.8}\text{Mg}_{0.2}\text{O}_3$ were checked by X-ray powder diffraction (DRON-6, Cu $K\alpha$ -radiation) supplied with a high-temperature attachment, HDK S1 (Edmund Buechler GmbH).

Neutron powder diffraction data on the $\text{Sr}_2\text{NiMoO}_6$ sample were collected with a D-7A diffractometer at the IVV-2M research reactor (Institute of Metal Physics, Russian Academy of Science, Yekaterinburg). The wavelength was $\lambda = 1.5155 \text{ \AA}$, the scan covered $10^\circ \leq 2\theta \leq 123^\circ$ range, and the step size was 0.05° .

The diffraction profiles were analyzed with the Fullprof Rietveld refinement program [9].

The resistance of the $\text{La}_{0.85}\text{Ba}_{0.15}\text{Mn}_{0.9}\text{Cr}_{0.1}\text{O}_3$ sample was measured by the four-probe technique at the partial oxygen pressures $P_{\text{O}_2} = 0.25 \text{ atm}$, $P_{\text{O}_2} = 10^{-3} \text{ atm}$, and $P_{\text{O}_2} = 10^{-6} \text{ atm}$ at 573–1273 K. The electric conductivity value σ was defined from sample resistance R measurements according to the equation:

$$\sigma = (l / S) \times R^{-1} \quad (1)$$

where l is the sample length at room temperature and S is the area of the cross-section of the sample.

The lengthening of the $\text{La}_{1-x}\text{Ba}_x\text{Mn}_{1-y}\text{Cr}_y\text{O}_3$ and $\text{Sr}_2\text{NiMoO}_6$ samples with temperature increase measurements were determined in a high-temperature dilatometer, NETZSCH DIL 402 C, at 293–1373 K with a heating and a cooling speed equal to 2 K/minute.

The isobaric linear coefficient of thermal expansion (LCTE) was defined from the dilatometry measurements and the X-ray data according to the equation

$$LCTE = \frac{1}{L_o} \left(\frac{\Delta L}{\Delta T} \right)_p = \frac{1}{3} \frac{1}{V_o} \left(\frac{\Delta V}{\Delta T} \right)_p \quad (2)$$

where L_o is the sample length at room temperature, ΔL is the current change of the length, V_o is the sample volume at room temperature, and ΔV is the current change of the sample volume.

Results and Discussion

Phase Relations in the $\text{LaMnO}_3\text{-BaMnO}_3\text{-BaCrO}_4\text{-LaCrO}_3$ System

In a solid solution formation study of $\text{La}_{1-x}\text{Ba}_x\text{Mn}_{1-y}\text{Cr}_y\text{O}_3$, the phase relations in air at 1373K in the $\text{LaMnO}_3\text{-BaMnO}_3\text{-BaCrO}_4\text{-LaCrO}_3$ quaternary oxide system were studied. It is important to note that phase relations in the $\text{LaMnO}_3\text{-BaMnO}_3\text{-BaCrO}_4\text{-LaCrO}_3$ oxide system have not been performed earlier in the whole composition range [10, 11].

According to the X-ray diffraction analysis, solid solutions of $\text{La}_{1-x}\text{Ba}_x\text{CrO}_3$ did not form in the binary $\text{LaCrO}_3\text{-BaCrO}_4$ system. This result differs from data [12] where the formation interval of solid solutions $\text{La}_{1-x}\text{Ba}_x\text{CrO}_3$ was reported to be $0.0 \leq x \leq 0.1$. $\text{La}_{0.95}\text{Ba}_{0.05}\text{CrO}_3$ and $\text{La}_{0.9}\text{Ba}_{0.1}\text{CrO}_3$ samples with a nominal composition contained two

phases: nondoped LaCrO_3 and orthorhombic BaCrO_4 .

The X-ray diffraction analysis of the samples with a nominal composition of $\text{La}_{1-x}\text{Ba}_x\text{Mn}_{1-y}\text{Cr}_y\text{O}_3$ showed that the $\text{La}_{0.95}\text{Ba}_{0.05}\text{Mn}_{0.8}\text{Cr}_{0.2}\text{O}_3$ sample was single-phase and had an orthorhombic structure and that the samples of $\text{La}_{0.85}\text{Ba}_{0.15}\text{Mn}_{0.9}\text{Cr}_{0.1}\text{O}_3$, $\text{La}_{0.85}\text{Ba}_{0.15}\text{Mn}_{0.8}\text{Cr}_{0.2}\text{O}_3$ and $\text{La}_{0.8}\text{Ba}_{0.2}\text{Mn}_{0.9}\text{Cr}_{0.1}\text{O}_3$ were single-phase and had a rhombohedral structure.

The room temperature lattice parameters of the $\text{La}_{1-x}\text{Ba}_x\text{Mn}_{1-y}\text{Cr}_y\text{O}_3$ solid solutions (the orthorhombic samples were calculated on the basis of the space group $Pnma$; the rhombohedral samples were calculated on the basis of the space group $R\bar{3}c$) are presented in Table 1. The decrease in the lattice parameters of the rhombohedral $\text{La}_{1-x}\text{Ba}_x\text{Mn}_{0.9}\text{Cr}_{0.1}\text{O}_3$ with the barium content increase was due to the formation of Mn^{4+} from Mn^{3+} ions during the replacement of La^{3+} ions with Ba^{2+} ions. According to [13], the ionic radius of Mn^{4+} (0.54 Å) was less than the ionic radius of Mn^{3+}_{HS} (0.65 Å) and Mn^{3+}_{LS} (0.58 Å). Tendency of lattice decreasing is more than tendency to increase the lattice caused by the replacement of some of the La^{3+} ions with the larger Ba^{2+} ions (the radii of the ions were 1.16 Å and 1.42 Å respectively).

Table 1
Room temperature lattice parameters of solid solutions
 $\text{La}_{1-x}\text{Ba}_x\text{Mn}_{1-y}\text{Cr}_y\text{O}_3$

x	y		a , Å	b , Å	c , Å	V , Å ³	R_{Bf}	R_f
0.05	0.2	<i>O</i>	5.4976(5)	7.8102(7)	5.5448(4)	238.08(4)	2.81	2.22
0.15	0.1	<i>R</i>	5.5495(3)	5.5495(3)	13.4407(8)	358.47(4)	0.822	0.677
0.15	0.2	<i>R</i>	5.5441(3)	5.5441(3)	13.4364(9)	357.67(4)	0.811	0.658
0.2	0.1	<i>R</i>	5.5392(5)	5.5392(5)	13.465(2)	357.80(7)	0.379	1.03

The X-ray diffraction analysis of the $\text{La}_{0.75}\text{Ba}_{0.25}\text{Mn}_{0.9}\text{Cr}_{0.1}\text{O}_3$ and $\text{La}_{0.8}\text{Ba}_{0.2}\text{Mn}_{0.7}\text{Cr}_{0.3}\text{O}_3$ samples with a nominal composition showed that these samples consisted of a rhombohedral perovskite phase $\text{La}_{1-x}\text{Ba}_x\text{Mn}_{1-y}\text{Cr}_y\text{O}_3$ and second-phase BaMnO_3 impurities. In contrast, the $\text{La}_{0.8}\text{Ba}_{0.2}\text{Mn}_{0.5}\text{Cr}_{0.5}\text{O}_3$ and $\text{La}_{0.9}\text{Ba}_{0.1}\text{Mn}_{0.2}\text{Cr}_{0.8}\text{O}_3$ samples with a nominal composition consisted of the rhombohedral and orthorhombic perovskite $\text{La}_{1-x}\text{Ba}_x\text{Mn}_{1-y}\text{Cr}_y\text{O}_3$ phases and third-phase BaCrO_4 impurities.

Our results obtained earlier (showing the existence of continuous $\text{LaMn}_{1-y}\text{Cr}_y\text{O}_3$ solid solutions [14] and the existence of $\text{La}_{1-x}\text{Ba}_x\text{MnO}_3$ solid solutions in the range $0.0 \leq x < 0.3$ [6]), together with the phase data on the $\text{La}_{1-x}\text{Ba}_x\text{Mn}_{1-y}\text{Cr}_y\text{O}_3$ samples in the present work, yielded a state diagram at 1373 K in air of the quaternary $\text{LaMnO}_3\text{-BaMnO}_3\text{-BaCrO}_4\text{-LaCrO}_3$ system (Fig. 1). Figure 1 shows the areas of rhombohedral (*R*) and orthorhombic (*O*) perovskite phases and $\text{La}_{1-x}\text{Ba}_x\text{Mn}_{1-y}\text{Cr}_y\text{O}_3$ formation.

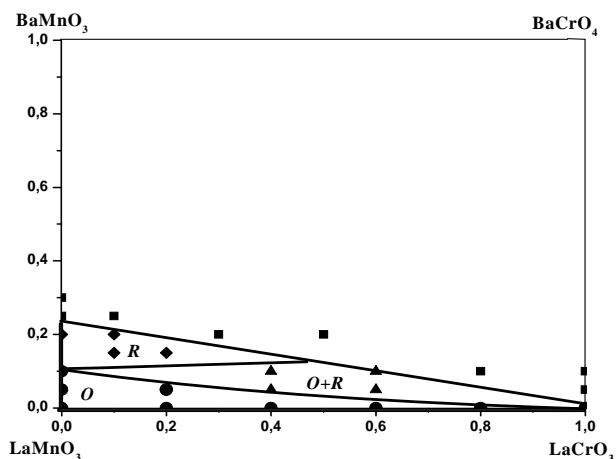


Fig. 1. Fragment of the state diagram of the quaternary system LaMnO_3 - BaMnO_3 - BaCrO_4 - LaCrO_3 .

Electric Conductivity and Thermal Expansion of $\text{La}_{1-x}\text{Ba}_x\text{Mn}_{1-y}\text{Cr}_y\text{O}_3$

As doped lanthanum-barium manganites can be used as cathode materials for SOFCs, electric conductivity measurements of the $\text{La}_{0.85}\text{Ba}_{0.15}\text{Mn}_{0.9}\text{Cr}_{0.1}\text{O}_3$ sample were performed. The linear size of the studied sample was $l = 1.827$ sm, $S = 0.4\text{sm}^2$. Figure 2 shows the dependences of the $\log \sigma$ vs $1000/T$ at $P_{\text{O}_2} = 0.25$ atm, $P_{\text{O}_2} = 10^{-3}$ atm, and $P_{\text{O}_2} = 10^{-6}$ atm at 573–1273 K.

As shown in Fig. 2, the conductivity of the sample increased in accordance with an increase in the temperature that specified to semiconductor conductivity. In comparison with the electroresistance measurements of the $\text{La}_{1-x}\text{Ba}_x\text{MnO}_3$ solid solutions [6], it is appeared that the substitution of Mn with Cr lead to a fall in the electrical conductivity of the base $\text{La}_{0.85}\text{Ba}_{0.15}\text{MnO}_3$. Possibly, this reduction was connected with charge disproportionation between the 3d-metals



$$K_1 = \frac{[\text{Cr}_{\text{Mn}}^{\prime}][\text{Mn}_{\text{Mn}}^{\times}]}{[\text{Mn}_{\text{Mn}}^{\prime}][\text{Cr}_{\text{Mn}}^{\bullet}]} \quad (4)$$

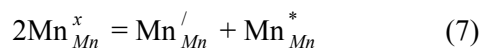
resulted in a decrease of the mobile charge carriers.

Electroneutrality condition was written now as:

$$[\text{Ba}_{\text{La}}^{\prime}] + [\text{Mn}_{\text{Mn}}^{\prime}] + [\text{Cr}_{\text{Mn}}^{\prime}] = [\text{Mn}_{\text{Mn}}^{\bullet}] + 2[\text{V}_{\text{O}}^{**}] + [\text{Cr}_{\text{Mn}}^{\times}] \quad (5)$$

$$K_2 = \frac{[\text{Mn}_{\text{Mn}}^{\bullet}][\text{V}_{\text{O}}^{**}]^2[\text{Cr}_{\text{Mn}}^{\times}]}{[\text{Ba}_{\text{La}}^{\prime}][\text{Mn}_{\text{Mn}}^{\prime}][\text{Cr}_{\text{Mn}}^{\prime}]} \quad (6)$$

From Fig. 2 oxygen partial pressure had a negligible effect on the sample conductivity owing to the dominant role of localized electrons and holes generation process for the account chrome and manganese ions disproportionation reactions (7) and (9):



$$K_3 = \frac{[\text{Mn}_{\text{Mn}}^{\prime}][\text{Mn}_{\text{Mn}}^{\bullet}]}{[\text{Mn}_{\text{Mn}}^{\times}]^2} \quad (8)$$



$$K_4 = \frac{[\text{Cr}_{\text{Mn}}^{\prime}][\text{Cr}_{\text{Mn}}^{\bullet}]}{[\text{Cr}_{\text{Mn}}^{\times}]^2} \quad (10)$$

where K_3 и K_4 equilibrium constants for reactions Eqs. (7) and (9) not depending on P_{O_2} .

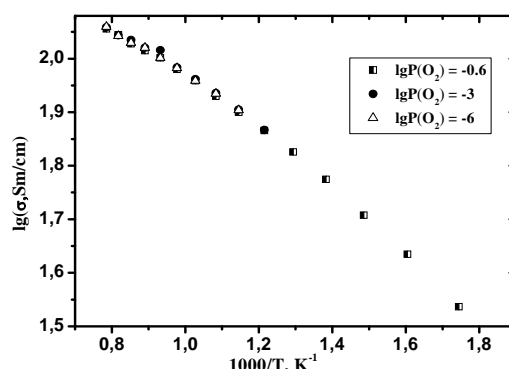


Fig. 2. Temperature dependences of $\text{La}_{0.85}\text{Ba}_{0.15}\text{Mn}_{0.9}\text{Cr}_{0.1}\text{O}_3$ sample electric conductivity at various partial oxygen pressures.

The calculation of the angle tangent of the dependences in Fig.2 showed that the average value of the activation energy $E_a = 0.076(1)$ eV was in the range characteristic for electro-migration proceeding via a small-radius polarons mechanism.

For the practical application of oxide materials as electrodes for SOFCs, it is important to estimate linear size changes of the study materials with temperature increase. In the present work, we studied the relative lengthening of the $\text{La}_{1-x}\text{Ba}_x\text{Mn}_{1-y}\text{Cr}_y\text{O}_3$ samples in air with temperature increases in the range of 293–1373 K at heating-cooling modes.

The average coefficients of thermal expansion calculated according to (2) are shown in Table 2. Based on these data, the thermal expansion coefficients of the investigated compounds at 303–1373 K appear to be close to those values of electrolyte materials based on zirconium dioxide doped with yttrium (YSZ), $10.8 \cdot 10^{-6} \text{ K}^{-1}$ [15], on the base $(\text{La}_{0.9}\text{Sr}_{0.1})_{0.98}\text{Ga}_{0.8}\text{Mg}_{0.2}\text{O}_3$, $11.1 \cdot 10^{-6} \text{ K}^{-1}$ [16], and on the base $\text{Ce}_{0.8}\text{Gd}_{0.2}\text{O}_2$, $11.5 \cdot 10^{-6} \text{ K}^{-1}$ [16]. Thus, these can be recommended as potential cathode materials for high-temperature elements.

Thermal and Chemical Compatibility of $\text{Sr}_2\text{NiMoO}_6$

Prospective anode materials for SOFCs based on double perovskites A_2MMoO_6 (Ca, Sr, Ba; M = Mg, Fe, Co, Ni, Zn) are attracting investigators' attention owing to their operating abilities at temperatures below 1073 K. Among the above mentioned oxides only Sr_2MMoO_6 (M = Co, Ni, Zn) may be synthesized directly in air [17]. Analyses of the published articles showed that crystal structure and the physical chemical properties of $\text{Sr}_2\text{NiMoO}_6$ sample were investigated mostly earlier [8,17-19] but despite this the existing data have not been consistent. According to [8, 19], $\text{Sr}_2\text{NiMoO}_6$ in air exhibits a homogenous tetragonal phase; however, according to [17, 18], $\text{Sr}_2\text{NiMoO}_6$ always contains an impurity phase, SrMoO_4 . By the way the presence SrMoO_4 in the synthesized sample put questions about stoichiometric composition of the sample. In the present work we decided to specify the phase composition of $\text{Sr}_2\text{NiMoO}_6$ sample with the neutron powder diffraction using necessity. Besides data on the temperature of the structure transition in $\text{Sr}_2\text{NiMoO}_6$ obtained earlier in [18] and [8] did not coincided pointing on 550 and 495 K correspondingly.

According to our X-ray diffraction data in the present work, $\text{Sr}_2\text{NiMoO}_6$ contained the impurity phase SrMoO_4 (in the amount of nearly 2 w.%) because of the presence in air of some Mo -ions in the +6 state. In addition, according to the neutron diffraction contained NiO (in the amount of nearly 2 weight %). Just neutron powder diffraction permitted to establish the accurate phase composition of the sample. Probably, the studied $\text{Sr}_2\text{NiMoO}_6$ powder consisted of NiO particles surrounding by the main phase granules. Owing to the fact that neutron scattering occurs not only from the sample surface but from the whole volume of

the sample, the neutron powder diffraction is more precious method. The presence of NiO in $\text{Sr}_2\text{NiMoO}_6$ can be explained by the stoichiometric composition of the starting powder. The main phase $\text{Sr}_2\text{NiMoO}_6$ was indexed on the base of the space group $I4/m$, with the tetragonal lattice parameters $a = 5.5497(2)$ and $c = 7.8956(5)$ Å. This finding is in good agreement only with [18]. However, $\text{Sr}_2\text{NiMoO}_6$ in [17] was indexed on the base of space group $I\bar{1}$ and in [19] space group was not specified yet.

The thermal compatibility of $\text{Sr}_2\text{NiMoO}_6$ with the electrolyte materials was studied by high-temperature X-ray diffraction ($298 \leq T, \text{K} \leq 533$) and dilatometry ($303 \leq T, \text{K} \leq 1373$) methods. Fig. 3 shows the temperature dependence of the pseudocubic cell volume of $\text{Sr}_2\text{NiMoO}_6$, and Fig. 4 shows the temperature dependences of the relative lengthening of $\text{Sr}_2\text{NiMoO}_6$.

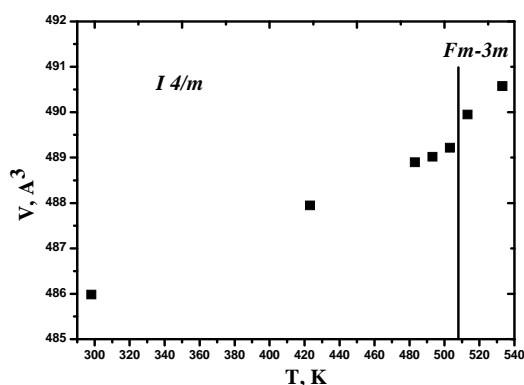


Fig. 3. Temperature dependence of the pseudocubic cell volume of $\text{Sr}_2\text{NiMoO}_6$ collected from high-temperature X-Ray data.

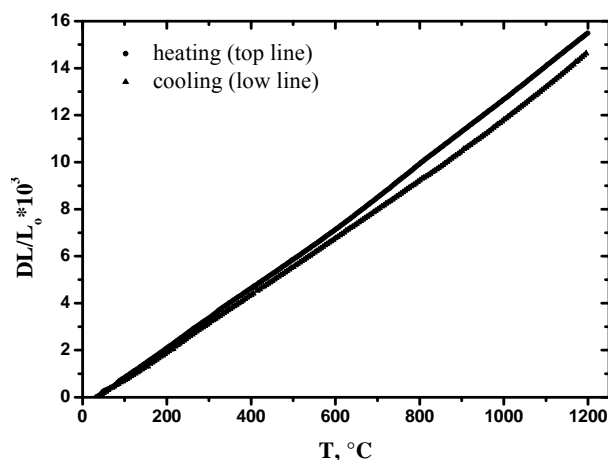


Fig. 4. Temperature dependences of the relative lengthening of $\text{Sr}_2\text{NiMoO}_6$ collected from dilatometry data obtained in heating-cooling regimes.

Figure 3 shows that at $T = 509$ K, the pseudocubic cell volume increased owing to the crystal phase transition from a tetragonal to a cubic phase. As seen in Fig. 4, this increase occurred at $T = 504$ and 513 K on the temperature dependence of the relative lengthening of $\text{Sr}_2\text{NiMoO}_6$ obtained in *heating* and *cooling* regimes, respectively. Thus, we concluded that the crystal phase transition from tetragonal to cubic in $\text{Sr}_2\text{NiMoO}_6$ occurs at a temperature nearly of 508 K. This result differs from that obtained earlier in neutron diffraction data [18] ($T = 550$ K) and that obtained for the relative lengthening of $\text{Sr}_2\text{NiMoO}_6$ ($T = 495$ K) [8]. The data difference must be occurred due to various rate of the sample heating, which is responsible for the equilibrium state reaching. In [18] the sample

heating rate was not noticed yet, whereas in [8] mode of data obtaining was not specified. Our result and result obtained in [8] are close owing to equal heating rate.

Table 2 shows the high-temperature X-ray diffraction and dilatometry data for the values of the average linear coefficients of thermal expansion of $\text{Sr}_2\text{NiMoO}_6$ obtained from Eq. (2). The values obtained for $\text{Sr}_2\text{NiMoO}_6$ LCTE at 303 - 847 K were in good agreement with data presented in [8] at 847 - 1373 K. Based on our data, we propose that the thermal expansion coefficients of $\text{Sr}_2\text{NiMoO}_6$ at 303 - 1373 K are close to those values of electrolyte materials. Thus, we propose that $\text{Sr}_2\text{NiMoO}_6$ may represent a potential anode material for high-temperature elements.

Table 2
Values of average linear coefficients of thermal expansion of potential electrode materials

composition	temperature range, K	CTE $\times 10^6$, K $^{-1}$
$\text{La}_{0.85}\text{Ba}_{0.15}\text{Mn}_{0.9}\text{Cr}_{0.1}\text{O}_3$	293-1373	12.8
$\text{La}_{0.85}\text{Ba}_{0.15}\text{Mn}_{0.8}\text{Cr}_{0.2}\text{O}_3$	293-1373	12.0
$\text{La}_{0.95}\text{Ba}_{0.05}\text{Mn}_{0.8}\text{Cr}_{0.2}\text{O}_3$	293-1373	12.0
$\text{Sr}_2\text{NiMoO}_6$ (dilatometry)	303-847	12.35
	847-1373	14.0
$\text{Sr}_2\text{NiMoO}_6$ (X-Ray)	298-533	12.38

In addition to the thermal compatibility of $\text{Sr}_2\text{NiMoO}_6$ with traditional electrolyte materials, we also studied its chemical compatibility. With this aim, $\text{Sr}_2\text{NiMoO}_6$ powder was ground in weight proportion 1:1 with powders of $\text{Ce}_{0.8}\text{Sm}_{0.2}\text{O}_{2-\delta}$, $\text{Zr}_{0.85}\text{Y}_{0.15}\text{O}_2$, and $(\text{La}_{0.9}\text{Sr}_{0.1})_{0.98}\text{Ga}_{0.8}\text{Mg}_{0.2}\text{O}_3$ respectively. The powders were annealed in air at 1073 K for 10 h and then at 1273 K for 20 h.

According to the X-ray diffraction data, $\text{Sr}_2\text{NiMoO}_6$ did not react with any of the electrolytes used at 1073 K, all patterns consisted of only $\text{Sr}_2\text{NiMoO}_6$ and electrolyte reflections. However the X-Ray patterns of the samples annealing at 1273 K showed that only $(\text{La}_{0.9}\text{Sr}_{0.1})_{0.98}\text{Ga}_{0.8}\text{Mg}_{0.2}\text{O}_3$ did not react with $\text{Sr}_2\text{NiMoO}_6$ at the same temperature. This result agrees with the result obtained in [8] where the chemical compatibility study was carried out at 1123 K. This finding suggests that $\text{Sr}_2\text{NiMoO}_6$ represents a very promising anode material for high-temperature elements.

Conclusions

In the present work, the perovskite phases of $\text{La}_{1-x}\text{Ba}_x\text{Mn}_{1-y}\text{Cr}_y\text{O}_3$ at 1373 K in air were defined on the basis of a phase relations study in the quaternary LaMnO_3 - BaMnO_3 - BaCrO_4 - LaCrO_3 system.

Based on electric conductivity measurements of $\text{La}_{0.85}\text{Ba}_{0.15}\text{Mn}_{0.9}\text{Cr}_{0.1}\text{O}_3$, we showed that substitution of *Mn* with *Cr* in $\text{La}_{1-x}\text{Ba}_x\text{MnO}_3$ saved the thermal compatibility of the cathode material with the electrolyte material but reduced the electric conductivity of the potential cathode material.

The average values of the thermal expansion coefficients of the potential cathode material $\text{La}_{1-x}\text{Ba}_x\text{Mn}_{1-y}\text{Cr}_y\text{O}_3$ and the potential anode material $\text{Sr}_2\text{NiMoO}_6$ were calculated from the dilatometry data. For $\text{Sr}_2\text{NiMoO}_6$, the crystal phase transition from a tetragonal to a cubic phase presence was established at nearly 508 K. We showed that $\text{Sr}_2\text{NiMoO}_6$ is compatible with

(La_{0.9}Sr_{0.1})_{0.98}Ga_{0.8}Mg_{0.2}O₃ as electrolyte material for SOFCs up to 1273 K.

This work was partly financially supported by the Russian Federal Agency on Science and Innovations and by the Russian Foundation for Basic Research (project № 11-03-00282-a).

References

1. Kawada, T., Mizusaki, J., in W. Vielstich et al. (ed.) *Handbook of Fuel Cells-Fundamentals, Technology and Application, Vol. 4: Fuel Cell Technology and Applications*, Wiley and Sons, Chichester, U.K., 2003, p 987.
2. Dokiya, M., *Solid State Ionics* 152:383 (2002).
3. MacIntosh, S., Gorte, R.J., *Chem. Rev.* 104:4845 (2004).
4. Ishihara, T., Masuda, H., Takita Y., *J. Am. Ceram. Soc.* 116:3801 (1994).
5. Cheng, J., Navrotsky, A., Zhou, X.-D., et al, *J. Mater. Res.* 20:191 (2005).
6. Voronin, V.I., Karkin, A.E., Petrov, A.N., et al, *Physica B* 234-236:710 (1997).
7. Cherepanov, V.A., Filonova, E.A., Voronin, V.I., et al., *J. Solid State Chem.* 153:205 (2000).
8. Wie, T., Ji, Y., Meng, X., et al., *Electrochem. Comm.* 10:1369 (2008).
9. Rodrigues-Carvajal, J. *Physica B* 192:55 (1993).
10. Hong, N., Hassini, A., Sakai, J., et al., *Mat. Sci. Eng.* 107:305 (2004).
11. Zhang, L., Xinbing, Chen, San Ping Jiang, et al., *Solid State Ionics* 180:1076 (2009).
12. Nedilko, S.A., Panchenko, G.V., *Ukrainian Chem. J.* 55:462 (1989).
13. Shannon, R.D., Prewitt, C.T., *Acta Cryst.* 25B:925 (1969).
14. Filonova, E.A., Demina, A.N., Petrov, A.N., *Russ. J. Neorg. Chem.* 52:771 (2007).
15. Laurencin, J., Delette, G., Morel, B. et al., *J. Power Sources* 192:344 (2009).
16. Tsipis, E. V., Kharton, V.V., Frade, J. R., *Electrochimica Acta* 52:4428 (2007).
17. Vasala, S., Lehtimäki, M., Huang, Y. H., et al., *J. Solid State Chem.* 183:1007 (2010).
18. Eriksson, A. K., Eriksson, S.-G., Ivanov, S. A., et al., *Mat. Res. Bull.* 41:144 (2006).
19. Gagulin, V.V., Korchagina, S. K., Ivanova, V. V., et al., *Inorg. Mater.* 39:625 (2003).

Received 26 October 2011